2-D Axisymmetric FEM-Based Approach for Identifying Dimension- and Frequency-Independent Material Parameters of Mn–Zn Ferrites

Reda Elkhadrawy[1], Joonas Vesa[1], Timo Tarhasaari[1], Vasiliki Tsakaloudi[2], and Paavo Rasilo[1]

[1]Electrical Engineering Unit, Tampere University, 33720 Tampere, Finland
[2]Laboratory of Inorganic Materials, Centre of Research and Technology Hellas, 57001 Thessaloniki, Greece

A 2-D axisymmetric finite element (FE) method (FEM)-based approach is presented for identifying intrinsic, dimension- and frequency-independent, electromagnetic material parameters of Mn–Zn ferrite cores. The parameters include the dc conductivity, complex permittivity, and complex permeability for both the grains and the grain-boundaries. The FE model is utilized for solving the full-wave electromagnetic field problem in a cross section of a ferrite core placed in a dielectric setting while accounting for the grain-scale microstructure. Dielectric impedance measurements are carried out for ferrite cores over a frequency range of 1 kHz–10 MHz. The intrinsic material parameters are identified by fitting the FE model parameters such that the modeled impedances match with the measured ones. A model with dimension- and frequency-independent electromagnetic material parameters is able to reproduce only the low-frequency behavior before the occurrence of dimensional resonance. In order to model the resonance behavior as well, a frequency-dependent term is introduced to the imaginary part of the reluctivity to account for "excess" magnetic losses.

Index Terms— **Complex permeability, complex permittivity, ferrites, finite element (FE) method (FEM), inverse problem.**

I. Introduction

MANGANESE–ZINC ferrite cores are generally made by sintering magnetic oxides (e.g., iron, manganese, and zinc oxides) doped with conductivity lowering additives such as calcium oxide and/or silicon dioxide [1], [2]. The sintering process results in a heterogeneous microstructure with conductive crystal grains and very resistive grain-boundaries where impurities are concentrated. This heterogeneity has an impact on the macroscopic electromagnetic characteristics of the material [3]. Due to the low losses that Mn–Zn ferrites offer, they are widely used in high-frequency power electronics applications [3], [4]. They also maintain high permittivity and high permeability which may cause dimensional effects at high frequency, especially in large cores. Dimensional effects are the reason that the apparent, or effective, material properties observable by impedance (voltage/current) measurements differ from the intrinsic properties which describe the local relationships between field quantities in the material [4]. Such effects make the task of directly measuring the intrinsic electromagnetic parameters, i.e., dc conductivity σ, complex permittivity $\varepsilon = (\varepsilon_r' - j\varepsilon_r'')\varepsilon_0$, and complex permeability $\mu = (\mu_r' - j\mu_r'')\mu_0$ a challenging task. Thus, inverse approaches are needed for identifying the intrinsic material parameters of ferrite cores. Better understanding of these parameters leads to more accurate power loss calculations and more reliable design process of power electronics devices based on ferrite cores.

The microstructure of a real core is extremely complex, and the material parameters are likely to vary locally both in the grains and the grain-boundaries. To define a local permeability and permittivity, it needs to be decided how the material is modeled. The definition of the permeability and permittivity depends on how the material microstructure is considered in the model. One approach is to model the material to be homogeneous with frequency-dependent parameters. Another approach is to model the heterogeneous structure by considering both the grains and the grain-boundaries. In the literature, the heterogeneous grain/grain-boundary structure of ferrite cores is often disregarded, and the material is assumed to be homogeneous with frequency- and dimension-dependent macroscopic parameters. Huang and Zhang [5] proposed an inverse approach for extracting the dimension-independent values of ε and μ of ferrite samples. Their approach was based on an analytical solution of the electric field in cuboid ferrite samples and iterating the parameter values based on the Newton–Raphson method. We recently presented a similar approach for toroidal samples based on the finite element (FE) method (FEM) and a nonlinear least-squares algorithm [6]. Although the approaches presented in [5] and [6] model the macroscopic behavior of the core efficiently, they do not consider the relation between the microstructure of the core and the macroscopic behavior. Moreover, the extracted material parameters from those approaches are frequency-dependent. The frequency-dependence in the macroscopic material parameters is related to the heterogeneous polycrystalline microstructure of the material, meaning that the frequency-dependent parameters of a homogenized sample are actually apparent parameters that describe the effective behavior of the grain/grain-boundary structure [7], [8]. Our hypothesis is that frequency-independent parameters are enough when the grain/grain-boundary structure is modeled. This has been investigated earlier through equivalent circuit models in [3], [9], and [10].

Manuscript received 29 February 2024; revised 15 May 2024; accepted 17 June 2024. Date of publication 20 June 2024; date of current version 26 September 2024. Corresponding author: R. Elkhadrawy (e-mail: reda.elkhadrawy@tuni.fi).

Color versions of one or more figures in this article are available at https://doi.org/10.1109/TMAG.2024.3417357.

Digital Object Identifier 10.1109/TMAG.2024.3417357

There are some approaches that investigate the eddy current losses in ferrite cores while accounting for the microstructure of the core. Dimier and Biela [9] made use of an RC equivalent circuit to model the apparent frequency-dependent ac conductivity and permittivity and calculated the eddy current losses based on analytical solutions of the fields in the ferrite core. Stenglein et al. [10] developed a macroscopic model for estimating the frequency-dependent effective material parameters by solving Maxwell's equations in the cross section of the core which can be used for calculating the eddy current losses in frequency and time domains. Fiorillo et al. [3] investigated the eddy current losses in ferrite cores in more detail by employing a multiscale approach.

The main drawback in all the aforementioned approaches that considered the heterogeneous structure of the core is that the electrical parameters, i.e., σ and ε for the grains and the grain-boundaries are identified based on modeling the ferrite core by an equivalent circuit approach. The equivalent circuit model consists of a series connection of two parallel RC pairs whose values are identified from dielectric measurements of only one ferrite sample that show no dimensional effects. Such an equivalent circuit might be sufficient to model a ferrite core only at low frequency when the core is free of any dimensional resonance effects. Another drawback of these approaches is that the grain permeability was not considered in the inverse solvers used for estimating the material parameters, but it was assumed to be equal to the initial measured permeability of the core. Such assumptions raise the questions of how the grain permeability affects the field solution in a ferrite core excited by an electric field at high frequency and if the grain permeability is actually equal to the measured macroscopic permeability.

The main goal of this work is to develop an FEM-based approach for identifying intrinsic, dimension- and frequency-independent, material parameters for both the grains and the grain-boundaries simultaneously with the ratio of the grain-boundary thickness and the grain width of the investigated Mn–Zn ferrite cores. In order to address the aforementioned drawbacks of the equivalent circuit approach, the electromagnetic field problem is solved based on Maxwell's equations while accounting for the permeability of the grains and the grain-boundaries. The inverse approach utilizes measurement data of two samples, the larger one showing dimensional resonance. The preparation process of the samples, the measurement setup, and the impedance measurements for the ferrite samples are presented in Section II. The computational models are also presented in Section II. Section III is devoted to the fitting results, investigating the uniqueness of the solution of the inverse problem and analysis of how the material parameters contribute to the impedance of the core. Section IV is dedicated to the discussion and conclusion.

II. Methods

A. Preparation Method of the Samples

Three Mn–Zn ferrite disks of the chemical formula $[Mn_{0.79}Zn_{0.21}]Fe_{2.1}O_4$ were prepared by the conventional ceramic processing of solid state synthesis. The mixed oxides of Fe_2O_3, MnO, and ZnO were prefired at 800 °C for 4 h. The prefired powder was doped with certain amounts of CoO, TiO_2, and CaO additives and milled for 9 h [2]. After drying and roll granulation of the resulting material with 0.2% of a polyvinyl alcohol binder, uniaxial compaction of three disks with outer diameter/height $(2R/d)$ of 22/7.5, 22/5, and 11/7 mm/mm, denoted by D1, D2, and D3, respectively, to a press density of 3.0 ± 0.1 g/cm^3 was performed. The ferrite specimens were sintered at 1300 °C for 3 h in an atmosphere-controlled kiln. The chemical composition of the ferrite was designed to exhibit an initial permeability $\mu_r' = 3000$ at 10 kHz in the sintered material.

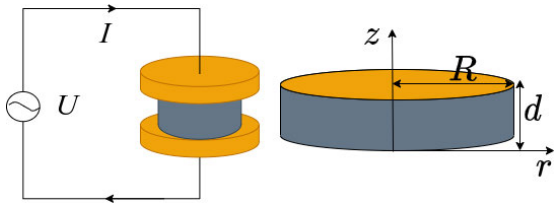

Fig. 1. Electrical circuit representation of dielectric impedance measurements (left) and the dimensions of a ferrite disk sample (right).

B. Dielectric Impedance Measurements

Small-signal dielectric impedance measurements were carried out at room temperature in the frequency range of 1 kHz–10 MHz with Novocontrol Alpha-A modular dielectric impedance measurement system in combination with ZG4 extension test interface and standard sample cell BDS1200 [12]. A sinusoidal voltage U is imposed across a sample placed between two 30 mm electrodes, and the total current I through the sample is measured according to Fig. 1 (left). The impedance of the sample is then calculated as a complex-valued function of the excitation frequency $\omega = 2\pi f$, $Z_{\text{meas}}(\omega) = U(\omega)/I(\omega)$. To get rid of the contact resistances, the top and bottom surfaces of the samples were coated with two layers of nickel and gold of thicknesses of 0.01 and 0.1 μm, respectively, using an electron beam evaporation setup. Moreover, before carrying out any measurements for the cores, open-circuit, short-circuit, and standard load calibrations of the measurement setup were performed in order to minimize uncertainties caused by the parasitic resistance and inductance of the measurement loop.

Ferrite cores prepared by the same manufacturing process share the same intrinsic material parameters with some tolerance defined by the quality of the sintering process, even when dimensional effects occur. On the other hand, the apparent properties observed by measurements are the same only until the occurrence of the dimensional effects [6]. Since the samples are excited by electric field, the phase angles shown in Fig. 2 first decrease when the frequency increases as the samples behave like imperfect capacitors. Also, it is clear from Fig. 2 that the samples share exactly the same apparent properties until the phase angles start to change direction and become dimension-dependent at about 200 kHz. That is because the magnetic field becomes more significant in the ferrite core and the dimensional effects start to occur. The

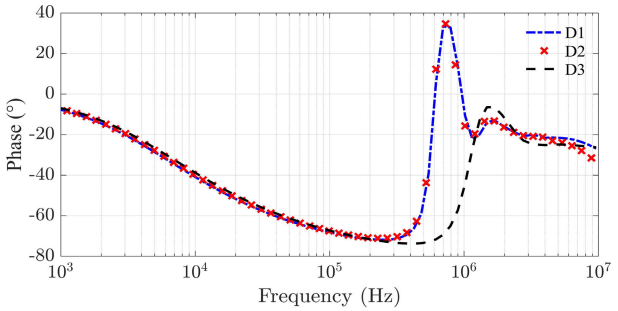

Fig. 2. Phase angle of the measured dielectric impedances for the Mn–Zn ferrite samples.

impedances of D1 and D2 have almost the same phase angle despite their height difference. Therefore, it can be assumed that only the magnitude of the impedance depends linearly on the height of the sample, and the field distribution is not affected by the height of the sample. The dimensional resonance behavior occurs when the phase angle is zero. Both D1 and D2 show dimensional resonance at about 600 kHz. In addition, the equivalence in the phase angles of D1 and D2 indicates that the intrinsic material properties of the cores are the same even with the occurrence of the dimensional effects.

C. Computational Models

Let us consider a ferrite core placed in a *dielectric* setting as shown in Fig. 1. The grain-scale microstructure of a ferrite sample prepared by the same chemical composition and sintering density as the measured ones is shown in Fig. 3 (left). Cylindrical coordinates r, φ, and z and frequency domain analysis are adopted. An axisymmetric 2-D model is chosen, which is justified by the facts the top and bottom of the sample are equipotential surfaces due to the electrodes and that the random grain structure makes the core macroscopically isotropic. This means that the φ-component of the current is zero on average. The axisymmetric model is thus considered to describe the average behavior of the fields in the sample. For modeling the grain/grain-boundary morphological inhomogeneity in the mirostructure of the ferrite core, a simplified regular array of grains is assumed, as shown in Fig. 3 (right). Due to the axisymmetry, the grains are thus modeled as homogeneous rings with a square cross section, but this is reasonable from the point-of-view of the currents, since they are confined in the rz plane. The flux density only has a circumferential component, and the permeability represents a homogenized value in the circumferential direction.

Considering the aforementioned conditions, the field problem can be solved only in one layer of grains in the axial direction and scaling the results with respect to the height of the whole sample. The magnetic field has only a circumferential component: $\boldsymbol{H} = H_\varphi(r, z)\hat{\varphi}$, where $\hat{\varphi}$ is the unit vector in the φ-direction. Moreover, the field variables are independent of φ. A 2-D axisymmetric FE model is constructed for solving the full-wave electromagnetic equation in a rectangular cross section of the core where $(r, z) \in [0, R] \times [0, \delta_g + 2\delta_b]$, where δ_g and δ_b are the grain width and the grain-boundary thickness, respectively. From Maxwell's equations,

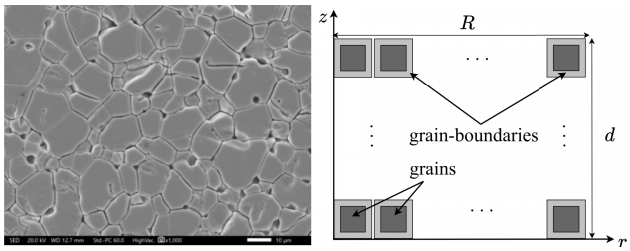

Fig. 3. Microscope image of the microstructure of a ferrite core and a simplified array of grains of the core rectangular cross section.

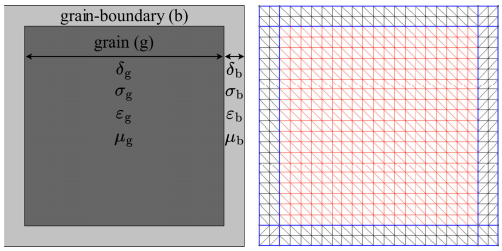

Fig. 4. Single grain/grain-boundary cell and its typical structured FE mesh. The grain-boundary thickness δ_b is exaggerated in the figure for visualization purposes.

the governing equation for the magnetic field strength $\boldsymbol{H}$ in a 2-D cross section of a disk core is

$$\nabla \times ((\sigma + j\omega\varepsilon)^{-1}\nabla \times \boldsymbol{H}) + j\omega\mu\boldsymbol{H} = 0$$
$$H_\varphi(0, z) = 0, \quad H_\varphi(R, z) = \frac{I}{2\pi R}. \tag{1}$$

Owing to the periodic grain structure in the z-direction and the fact that the grain is positioned vertically in the middle of the modeling domain and surrounded from both sides by half of the boundary thickness as shown in Fig. 4 (left), homogeneous Neumann conditions can be used on the top and bottom boundaries of the modeling domain.

The above choices of the modeling domain and the boundary conditions neglect the displacement current between the electrodes outside of the disk sample. It was experimentally confirmed that using 40 mm electrodes instead of 30 mm ones did not change the measured impedance. In addition, the numerical simulations in [6] showed that considering the displacement current in the middle of toroidal cores did not affect the field distributions in the cores. Thus, the effect of the air region is considered to be negligible.

It was observed that the dimensional effects in a single grain/grain-boundary cell are negligible, and thus, the field distribution in the cell is affected only by the ratio of the boundary thickness and grain width $\zeta = (\delta_b/\delta_g)$, and not the actual dimensions. Therefore, only the relative boundary thickness ζ is identified, and the grain width δ_g is fixed to a predefined value. Let $\Lambda = [\zeta, \sigma_g, \varepsilon_g, \mu_g, \sigma_b, \varepsilon_b, \mu_b]$ be a vector containing both the size and the electromagnetic material parameters of the grains (subscript g) and the grain-boundaries (b). The impedance is calculated as

$$Z_{\text{cal}}(\omega, \Lambda) = \frac{1}{|I|^2}\int \left[(\sigma + j\omega\varepsilon)^{-1}\|\nabla \times \boldsymbol{H}\|^2 + j\omega\mu\|\boldsymbol{H}\|^2\right]d\Omega. \tag{2}$$

For identifying the intrinsic parameters Λ, the inverse problem is formulated as an optimization problem [16]

$$\Lambda = \text{argmin}_{\Lambda} \sum_{i=1} \frac{|Z_{\text{meas}}(\omega_i) - Z_{\text{cal}}(\omega_i, \Lambda)|^2}{|Z_{\text{meas}}(\omega_i)|^2} \tag{3}$$

where i sums over the measured frequencies. Equation (1) is discretized with the Galerkin FEM with nodal elements for H_φ and combined with a nonlinear least-squares algorithm for solving (3) such that the calculated impedances match with the measured values. Following the results of [14] and [15], a structured FE mesh with right-angled triangular elements is used to avoid numerical problems related to the large aspect ratio of the elements in the grain-boundaries as shown in Fig. 4 (right).

The real part of the impedance causes the losses, and the imaginary part contributes to the reactive power. The total losses comprise dc and eddy-current conduction losses, dielectric hysteresis losses described by the imaginary part of the permittivity, as well as the magnetic hysteresis and excess losses described by the frequency-independent and frequency-dependent terms in the imaginary part of the permeability, respectively. Dividing the impedance into an equivalent series resistance and reactance as $Z_{\text{cal}} = R_{\text{cal}} + jX_{\text{cal}}$, the different contributions of the parameters to R_{cal} and X_{cal} can be separated by

$$R_\sigma = \frac{\int \sigma \|\boldsymbol{E}\|^2 d\Omega}{|I|^2} \tag{4}$$

$$R_{\varepsilon''} = \frac{\int \omega\varepsilon'' \|\boldsymbol{E}\|^2 d\Omega}{|I|^2} \tag{5}$$

$$R_{\mu''} = \frac{\int \omega\mu'' \|\boldsymbol{H}\|^2 d\Omega}{|I|^2} \tag{6}$$

$$X_{\varepsilon'} = -\frac{\int \omega\varepsilon' \|\boldsymbol{E}\|^2 d\Omega}{|I|^2} \tag{7}$$

$$X_{\mu'} = \frac{\int \omega\mu' \|\boldsymbol{H}\|^2 d\Omega}{|I|^2} \tag{8}$$

where $\boldsymbol{E} = (\sigma + j\omega\varepsilon)^{-1} \nabla \times \boldsymbol{H}$. These components correspond to the resistive loss, dielectric loss, hysteresis and excess loss, capacitive reactive power, and inductive reactive power, respectively.

III. Results

A. Parameter Identification

Since D1 and D2 show similar behavior in the whole frequency range as shown in Fig. 2, the impedance measurements of only D1 and D3 were used with the inverse approach presented in Section II for identifying all the electromagnetic material parameters and the relative boundary thickness simultaneously. Although only dielectric measurements where the ferrite cores act as capacitors are considered, the occurrence of dimensional effects makes it possible to identify also the magnetic parameters, i.e., the complex permeability of the grains and grain-boundaries.

Making use of the microscope image, δ_g is set to be equal to the average grain size which is 11 μm, and a lower bound of zero is set to all identified parameters in Λ to ensure physically reasonable values. The inverse approach is employed, and a parameter set Λ_1 is identified and depicted in Table I. The identified parameters agree with the literature such that the inductive grains are conducting and the capacitive grain-boundaries have high resistivity. The measured and fitted impedances of the ferrite cores used for identifying the parameter set Λ_1 are shown in Fig. 5, and they agree in the sense that they have the same trend only in the low-frequency region, i.e., before the dimensional resonance occurs. It can be seen from Fig. 5 (right) that X_{cal} for both D1 and D3 becomes positive and keeps increasing after 1 MHz while the measured values are positive only around the resonance peak. Since the core is modeled while placed in a dielectric setting, such increase in X_{cal} must come from inductive effects, i.e., the grain permeability. D1 shows strong resonance behavior around 600 kHz, so the grain permeability must have a significant effect on the impedance around 600 kHz.

Theoretically, the total power losses in a ferrite inductor, i.e., a ferrite core placed in an inductive setting could be separated into three contributions with quite different physical origins, i.e., hysteresis, eddy-current, and excess losses. The physical origin of the excess loss is still somewhat unclear. However, magnetic resonance processes, which are linked to the imaginary part of the permeability, are claimed to be responsible for the excess losses [17], [18]. In other words, the permeability of ferrite cores shows some relaxation behavior at high frequency, which is usually attributed to the excess losses [3], [19]. Moreover, it is not clear in the literature how the permeability of a single grain behaves at high frequency. Although the problem and the measurements are in a dielectric setting, the permeability has a significant effect on the measurements at high frequency around the resonance region. Therefore, we introduce an additional term to represent some excess magnetic losses for the grains by adding a frequency-dependent imaginary part to the grain reluctivity as

$$\frac{1}{\mu_g} = \frac{1}{\mu_g' - j\mu_g''} + jcf^\alpha. \tag{9}$$

The inverse approach was repeated with the proposed modification of μ_g, and a new parameter set Λ_2 was identified by fixing $\alpha = 0.5$. Λ_2 is depicted in Table I, and the measured and fitted impedances of the ferrite cores used for identifying Λ_2 are shown in Fig. 6. The fitted impedances follow the same trend as the measured ones over the whole frequency range as shown in Fig. 6. The resonance behavior in the samples is now captured in the fitted impedances in the MHz region. It can also be noticed from Fig. 6 (right) that X_{meas} and X_{cal} have the same trend over the whole frequency range, especially during and after the resonance behavior. The new parameters of Λ_2 differ from the corresponding ones of Λ_1 in the range of 50%–150% except the grain parameters σ_g, ε_g'', and μ_g'' that contribute to the resistive losses. σ_g and μ_g'' have increased by factors of 11.5 and 6, respectively, but ε_g'' has decreased to be 0. The forward problem (1–2) depends on σ_b much more than σ_g as $\delta_b/\sigma_b \approx 5 \times 10^{-5}$ (m^2/S) $\gg \delta_g/\sigma_g \approx 3 \times 10^{-8}$ (m^2/S), which explains why the fitting in the low-frequency region has

TABLE I

INTRINSIC MATERIAL PARAMETERS FOR THE Mn–Zn FERRITE SAMPLES. Λ_1 AND Λ_2 ARE IDENTIFIED WITHOUT AND WITH AN ADDITIONAL EXCESS LOSS TERM, RESPECTIVELY

Parameter Set	Region	σ (S/m)	ε_r'	ε_r''	μ_r'	μ_r''	c ($\mathrm{Hz}^{-\alpha}\mathrm{m/H}$)	α	ζ
Λ_1	Grains	28.7	1.4	3.5	2100	0.2	-	-	6.2×10^{-5}
	Boundaries	1.5×10^{-5}	21.5	4.4	1	17.8	-	-	
Λ_2	Grains	351	1.1	0	2443	0.3	11.1×10^{-2}	0.5	8.3×10^{-5}
	Boundaries	2×10^{-5}	21.7	3.1	1.2	7.2	-	-	

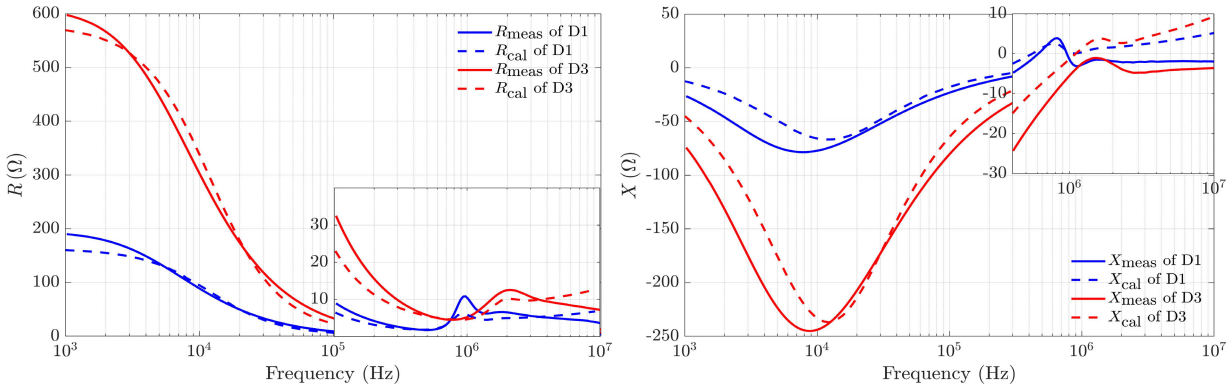

Fig. 5. Measured and fitted impedances for the Mn–Zn ferrite samples using the parameter set Λ_1, R_{cal} (left), and X_{cal} (right).

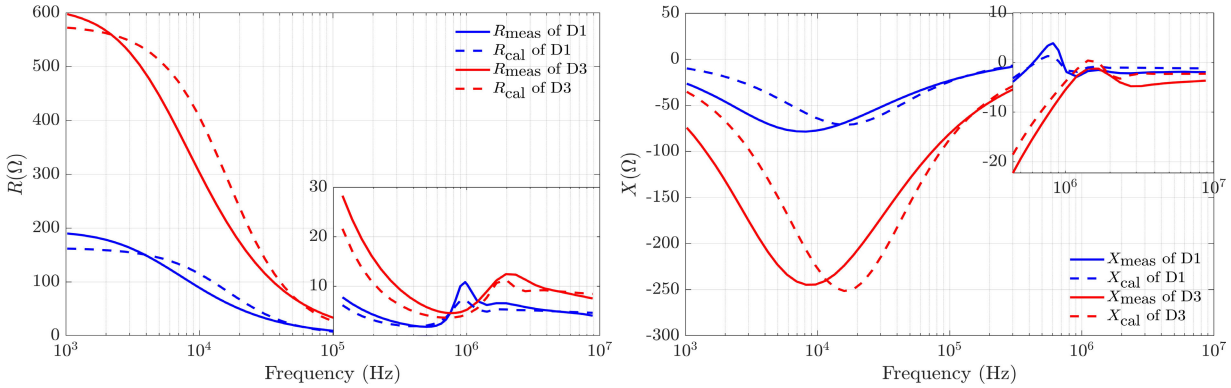

Fig. 6. Measured and fitted impedances for the Mn–Zn ferrite samples using the parameter set Λ_2, R_{cal} (left), and X_{cal} (right).

not changed much from Λ_1 to Λ_2 despite the large increase of σ_g. The effects due to the increase of μ_g'' might be compensated by the ones due to the decrease of ε_g''. There are still some discrepancies between the measured and fitted impedances, especially in the low-frequency region. Such discrepancies might be caused by porosity and random grain structure in the actual samples, which were not considered in the model.

B. Uniqueness of the Inverse Problem

As explained in Section II-C, the field solution in a single grain is only affected by the relative boundary thickness ζ, not the real dimensions δ_g and δ_b, and thus, only ζ was included in the identified parameters Λ instead of both δ_g and δ_b. Nevertheless, it was observed that the solution of (3) might still not be unique, and several combinations of Λ could yield the same macroscopic impedance of the core. To investigate other possible parameter combinations, the inverse approach was repeated while fixing the relative boundary thickness to different values in the range of 70%–130% of ζ identified in Λ_2 which will be denoted by $\zeta_2 = 8.3 \times 10^{-5}$. Moreover, Λ_2 was used as initial values for the nonlinear least-squares algorithm. The rest of the parameters are identified and shown in Fig. 7. The fitted impedances for different relative boundary thicknesses are shown in Fig. 8. Although the relative boundary thickness and the identified parameters change significantly, all the fitted impedances are very close to each other. It seems that there are interdependences between some material parameters in the sense that the effect of one parameter on the macroscopic behavior compensates the effect of another. In other words, several combinations of the parameter set Λ could be identified depending on the relative boundary thickness. It can be seen from Fig. 7 that the parameters σ_b, ε_b', and ε_b'' increase more or less linearly with increasing relative boundary thickness. In the other parameters, the variation is less systematic, but also smaller.

C. Loss and Power Separation

The material parameters contribute differently to the dielectric impedance of the core and consequently to the power loss and reactive power. The impedances of D1 and D3 are calculated with the parameter set Λ_2, and the real and

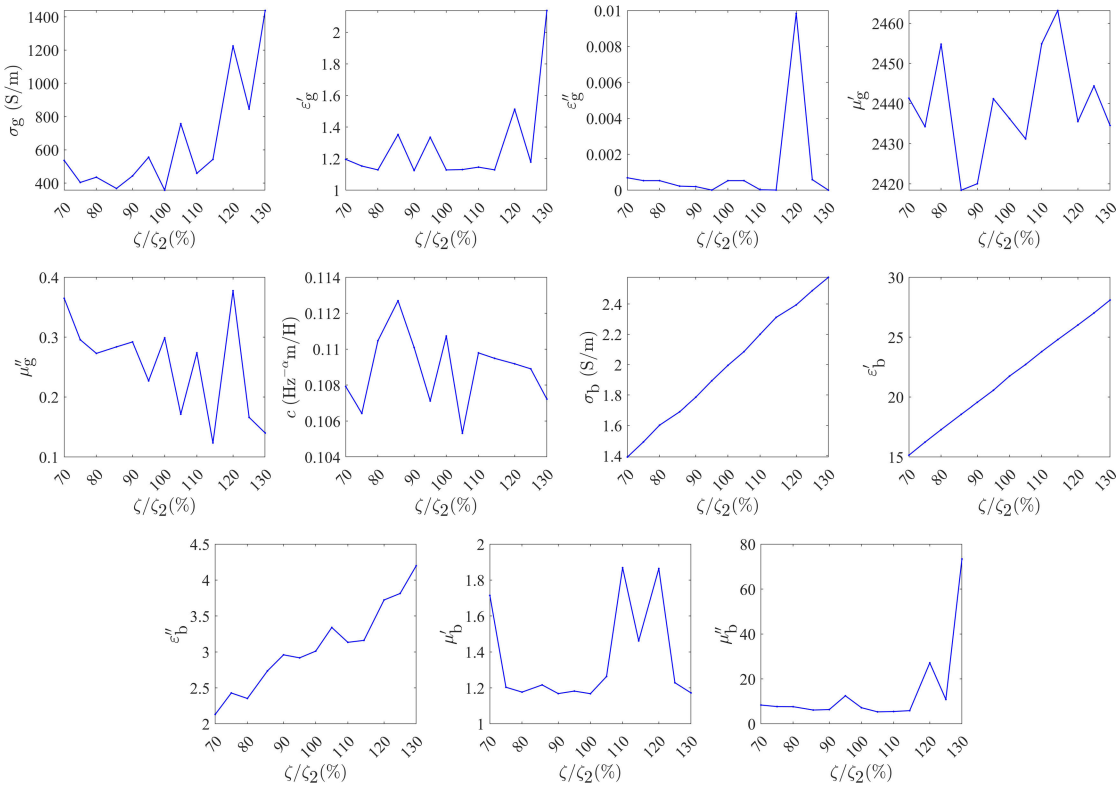

Fig. 7. Change of fitted parameters while fixing the relative boundary thickness ζ to a constant value in the range of 70%–130% of ζ_2 (ζ in Λ_2).

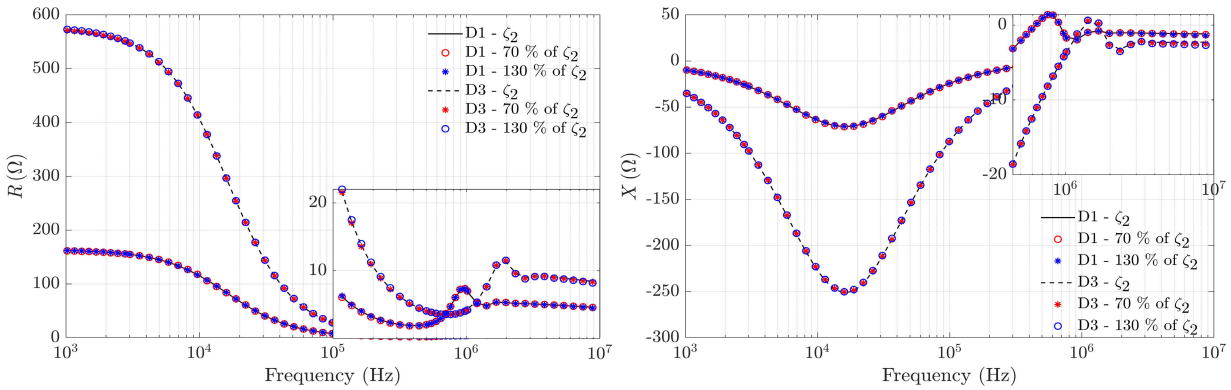

Fig. 8. Fitted impedances while fixing the relative boundary thickness ζ to a constant value in the range of 70%–130% of ζ_2, R_{cal} (left), and X_{cal} (right).

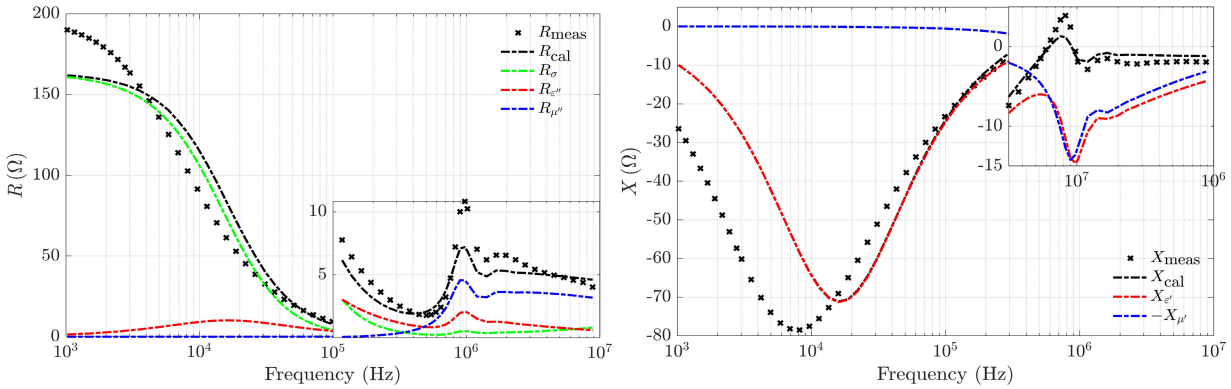

Fig. 9. Impedance of D1 calculated using the parameter set Λ_2 and separated into different components of R_{cal} (left) and X_{cal} (right).

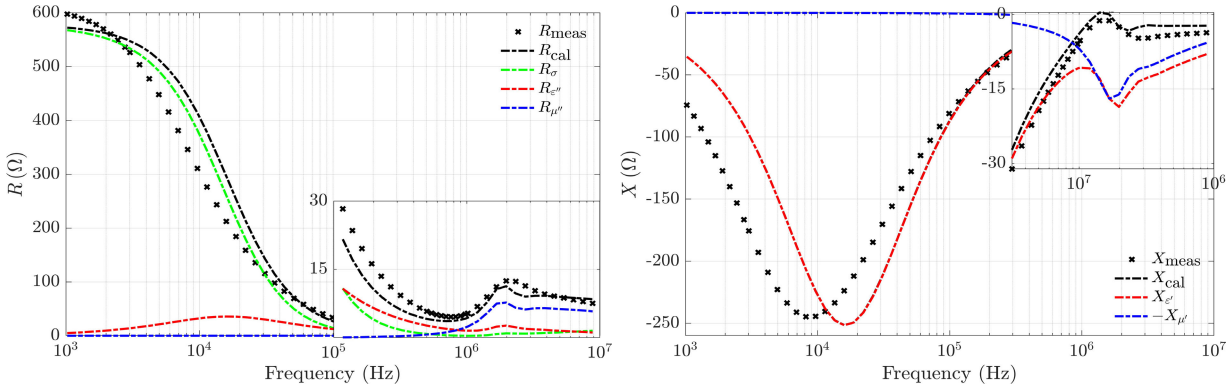

Fig. 10. Impedance of D3 calculated using the parameter set Λ_2 and separated into different components of R_{cal} (left) and X_{cal} (right).

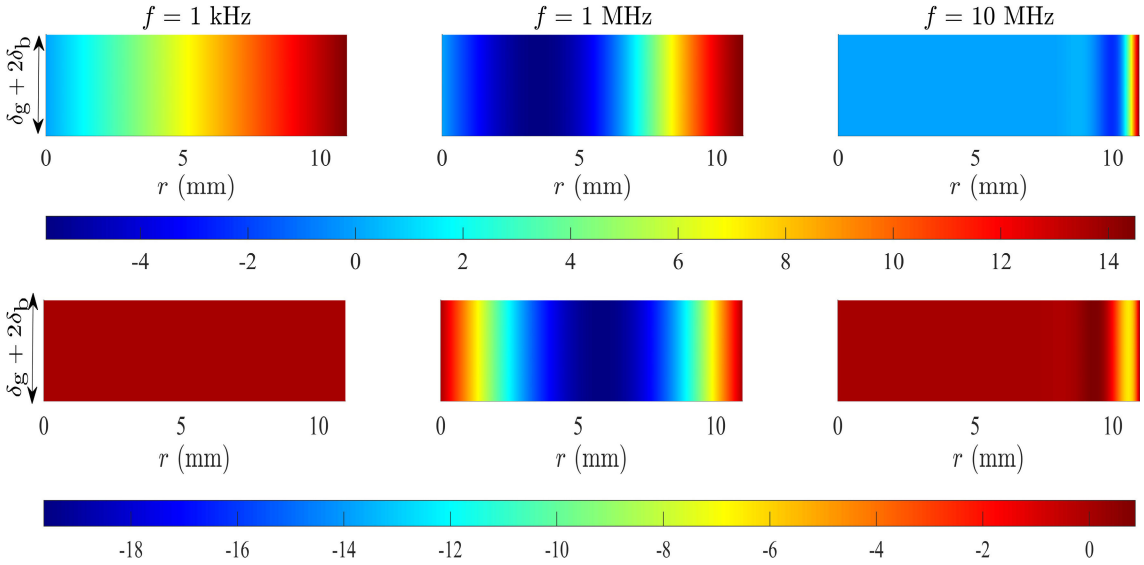

Fig. 11. Real (top) and imaginary (bottom) parts of the magnetic field strength H_φ (A/m) in one layer of grains in the axial direction for D1 using the parameter set Λ_2 and $I = 1$ A at 1 kHz, 1 MHz, and 10 MHz. The height is exaggerated in the figure for visualization purposes.

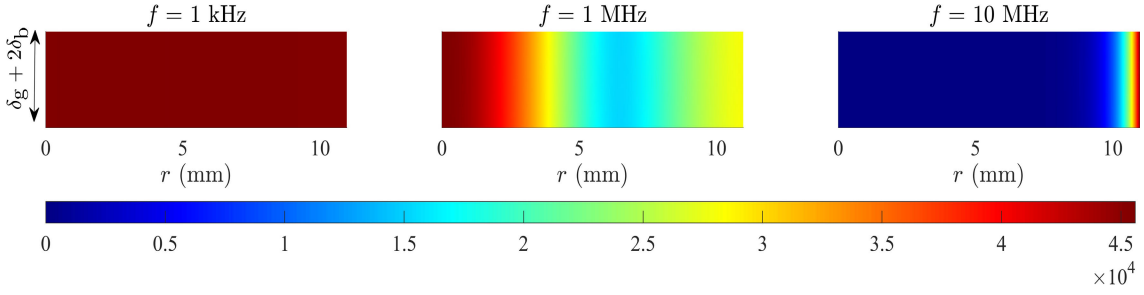

Fig. 12. Field plots of the total current density $||\nabla \times \boldsymbol{H}||$ (A/m^2) in one layer of grains in the axial direction for D1 using the parameter set Λ_2 and $I = 1$ A at 1 kHz, 1 MHz, and 10 MHz. The height is exaggerated in the figure for visualization purposes.

imaginary parts of the impedances are separated into different contributions by (4)–(8), as shown in Figs. 9 and 10. The resistive loss represented by R_σ is the main contributor to the total loss R_{cal} below 50 kHz, and the dielectric loss $R_{\varepsilon''}$ contributes significantly above 20 kHz as shown in Fig. 9 (left). The hysteresis and excess loss $R_{\mu''}$ contributes only in the high-frequency region, i.e., above 300 kHz. Considering that the core is placed in a dielectric setting, the capacitive reactive power $X_{\varepsilon'}$ is more dominant than the inductive reactive power $X_{\mu'}$ as shown in Fig. 9 (right). However, the magnetic field increases with frequency, and $X_{\mu'}$ becomes comparable to $X_{\varepsilon'}$ around 600 kHz which causes the dimensional resonance. The different contributions of the material parameters to R_{cal} and X_{cal} of the impedance of D3 show similar behavior as D1, except that D3 does not show strong dimensional resonance as D1.

Another way to study how the permeability affects the dielectric measurements is to visualize the distribution of the magnetic field in the core at different frequencies. The FE model illustrated in Section II-C is used for solving the

magnetic field strength H_φ (A/m) in one layer of grains in the axial direction for D1 using the parameter set Λ_2 and $I = 1$ A at 1 kHz, 1 MHz, and 10 MHz. Field plots of the magnetic field H_φ (A/m) and the total current density $||\nabla \times \boldsymbol{H}||$ (A/m^2) are shown in Figs. 11 and 12, respectively. At 1 kHz, the real part of H_φ decreases from its maximum value at the outer boundary toward the center of the core, which agrees with the fact that the current is evenly distributed along the radius. The imaginary part of H_φ is almost zero in the whole core. As the frequency increases, the concentration of the real part of H_φ moves toward to the outer boundary of the core. At 1 MHz, the imaginary part is more significant, and it is concentrated around $r = R/2$. Furthermore, it can be seen from Fig. 12 that the current distribution becomes less uniform as the frequency increases. At 10 MHz, the current tends to pass only through the outer surface of the core.

IV. Discussion and Conclusion

An inverse approach based on a 2-D axisymmetric FE model is presented for identifying the intrinsic material parameters of ferrite cores placed in a dielectric setting. The solution of the inverse problem (3) is not unique, and several combinations of intrinsic material parameters can be identified depending on the considered dimensions of the grains and grain-boundaries, more specifically the relative boundary thickness. Therefore, microscope images of the core microstructure are needed to provide realistic range for the grain size. The permeability has a significant effect on the dielectric behavior of ferrite cores at high frequency, and it causes dimensional effects especially in large cores. A frequency-dependent imaginary term was added to the grain reluctivity to represent excess losses and to capture the resonance behavior in the fitting results. The material parameters affect the dielectric behavior of the ferrite core in different manners, and consequently also the core losses. The proposed model could be used as a tool for predicting the dielectric behavior of ferrite cores. Modeling the samples' porosity and the random distribution of the grains might improve the reliability of the proposed model.

Acknowledgment

This project has received funding from the European Research Council (ERC) under the European Union's Horizon 2020 research and innovation programme (grant agreement No 848590). The Academy of Finland is also acknowledged for financial support (grants No 326485 and 346440).

References

[1] C. Beatrice, S. Dobák, V. Tsakaloudi, F. Fiorillo, A. Maniudaki, and V. Zaspalis, "Magnetic aging in TiO_2-doped Mn–Zn ferrites," *J. Magn. Magn. Mater.*, vol. 502, May 2020, Art. no. 166576.

[2] V. Tsakaloudi and V. Zaspalis, "Synthesis of a low loss Mn–Zn ferrite for power applications," *J. Magn. Magn. Mater.*, vol. 400, pp. 307–310, Feb. 2016.

[3] F. Fiorillo, C. Beatrice, O. Bottauscio, and E. Carmi, "Eddy-current losses in Mn-Zn ferrites," *IEEE Trans. Magn.*, vol. 50, no. 1, pp. 1–9, Jan. 2014.

[4] S. Lin, T. Brinker, L. Fauth, and J. Friebe, "Review of dimensional resonance effect for high frequency magnetic components," in *Proc. EPE ECCE*, Genova, Italy, Sep. 2019, pp. P.1–P.10.

[5] R. Huang and D. Zhang, "Experimentally verified Mn–Zn ferrites' intrinsic complex permittivity and permeability tracing technique using two ferrite capacitors," *IEEE Trans. Magn.*, vol. 43, no. 3, pp. 974–981, Mar. 2007.

[6] R. Elkhadrawy, J. Panchal, T. Tarhasaari, K. Lahti, and P. Rasilo, "1-D FEM-based approach for extracting dimension-independent material properties of mn-zn toroidal ferrite cores," *IEEE Trans. Magn.*, vol. 58, no. 9, pp. 1–4, Sep. 2022.

[7] A. Marjamäki, R. Schneckenleitner, R. Elkhadrawy, and P. Rasilo, "High-frequency modeling of granular soft magnetic materials with local model order reduction," *IEEE Trans. Magn.*, vol. 60, no. 3, pp. 1–4, Mar. 2024.

[8] O. Bottauscio, M. Chiampi, and A. Manzin, "Multiscale modeling of heterogeneous magnetic materials," *Int. J. Numer. Model., Electron. Netw., Devices Fields*, vol. 27, no. 3, pp. 373–384, Sep. 2013.

[9] T. Dimier and J. Biela, "Eddy current loss model for ferrite ring cores based on a meta-material model of the core properties," *IEEE Trans. Magn.*, vol. 58, no. 2, pp. 1–5, Feb. 2022.

[10] E. Stenglein, H. Rossmanith, and M. Albach, "Macroscopic modeling of MnZn ferrites for the calculation of eddy-current losses in the frequency- and time-domain," in *Proc. COMPEL*, Padua, Italy, Jun. 2018, pp. 1–7.

[11] V. Loyau, G.-Y. Wang, M. L. Bue, and F. Mazaleyrat, "An analysis of mn-zn ferrite microstructure by impedance spectroscopy, scanning transmission electron microscopy and energy dispersion spectrometry characterizations," *J. Appl. Phys.*, vol. 111, no. 5, pp. 05392:1–05392:9, Mar. 2012.

[12] (Feb. 2022). *Alpha-A Modular Dielectric/Impedance Measurement System Mainframes*. [Online]. Available: https://www.novocontrol.de/php/ana_alpha_main.php

[13] A. Stadler, M. Albach, and A. Bucher, "Calculation of core losses in toroids with rectangular cross section," in *Proc. EPE-PEMC*, Portoroz, Slovenia, Aug. 2006, pp. 828–833.

[14] J. Shewchuk, "What is a good linear finite element? Interpolation, conditioning, anisotropy, and quality measures," in *Proc. 11th Int. Meshing Roundtable*, Ithaca, NY, USA, Sep. 2002.

[15] P. Rasilo, J. Vesa, and J. Gyselinck, "Electromagnetic modeling of ferrites using shell elements and random grain structures," *IEEE Trans. Magn.*, vol. 56, no. 2, pp. 1–4, Feb. 2020.

[16] J. Mueller and S. Siltanen, *Linear and Nonlinear Inverse Problems With Practical Applications* (Computational Science & Engineering). Philadelphia, PA, USA: Society for Industrial and Applied Mathematics, 2012.

[17] W. H. Jeong, Y. H. Han, and B. M. Song, "Effects of grain size on the residual loss of Mn–Zn ferrites," *J. Appl. Phys.*, vol. 91, no. 10, pp. 7619–7621, May 2002.

[18] W. H. Jeong, B. M. Song, and Y. H. Han, "Analysis of power losses in Mn–Zn ferrites," *Jpn. J. Appl. Phys.*, vol. 41, pp. 2912–2915, May 2002.

[19] F. Fiorillo, C. Beatrice, O. Bottauscio, A. Manzin, and M. Chiampi, "Approach to magnetic losses and their frequency dependence in Mn–Zn ferrites," *Appl. Phys. Lett.*, vol. 89, no. 12, pp. 122513:1–122513:3, Sep. 2006.